TRANSONIC FLUTTER CALCULATIONS USING THE EULER EQUATIONS

Oddvar O. Bendiksen
Kenneth A. Kousen
Princeton University, Princeton, NJ

UNSTEADY EULER EQUATIONS

In transonic flutter problems where shock motion plays an important part, it is believed that accurate predictions of the flutter boundaries will require the use of codes based on the Euler equations. Only Euler codes can obtain the correct shock location and shock strength, and the crucially important shock excursion amplitude and phase lag. (For a discussion of the importance of shocks in transonic flutter, see Ref. 1.) The present study is based on the finite volume scheme developed by Jameson and Venkatakrishnan (Refs. 2,3) for the two-dimensional unsteady Euler equations. The equations are solved in integral form on a moving mesh, Eqs. (1-2). Here the variables p, ρ, u, v and e are the pressure, density, cartesian velocity components, and total energy, respectively, and x_t and y_t are the velocity components of the moving boundary $\partial\Omega$ of an element Ω. By applying Eq. (1) to each element or cell (i,j), a system of ordinary differential equations is obtained, Eqs. (3), where S_{ij} is the cell area, Q_{ij} is the net flux out of the cell, and D_{ij} represents dissipative terms added to damp numerical oscillations (see Refs. 3,4). A five-stage Runge-Kutta scheme is used to integrate Eqs. (3) forward in time.

FINITE VOLUME FORMULATION

- **INTEGRAL FORM ON A MOVING MESH**

$$\frac{\partial}{\partial t}\iint_{\Omega} W\,dx\,dy + \int_{\partial\Omega} (f\,dy - g\,dx) = 0 \qquad (1)$$

$$W = \begin{Bmatrix} \rho \\ \rho u \\ \rho v \\ \rho e \end{Bmatrix}, \quad f = \begin{Bmatrix} \rho(u-x_t) \\ \rho u(u-x_t)+p \\ \rho v(u-x_t) \\ \rho e(u-x_t)+pu \end{Bmatrix}, \quad g = \begin{Bmatrix} \rho(v-y_t) \\ \rho u(v-y_t) \\ \rho v(v-y_t)+p \\ \rho e(v-y_t)+pv \end{Bmatrix} \qquad (2)$$

- **DISCRETIZED FORM WITH DISSIPATION, ADAPTIVE OR TVD-BASED**

$$\frac{d}{dt}(S_{ij}W_{ij}) + Q_{ij} - D_{ij} = 0 \qquad (3)$$

TYPICAL SECTION MODEL

The wing is modeled as a typical section, with two degrees of freedom (bending h and torsion α), as illustrated in Fig. 1. The usefulness of this model in capturing the fundamental features of bending-torsion flutter is by now well established. In the usual notation, the equations of motion are of the form given by Eqs. (5) and (6), where the lift and moment coefficients C_L and C_M depend on the motion of the airfoil. Because we will consider finite (rather than infinitesimal) amplitude motion, the superposition principle cannot be used. In the present study, C_L and C_M are calculated numerically from the unsteady pressure coefficient on the airfoil surface at the end of each time interval, obtained from the numerical solution of the Euler equations. It should be emphasized that the equations of motion are nonlinear through the dependence of C_L and C_M on the motion h,α of the airfoil (and its time history).

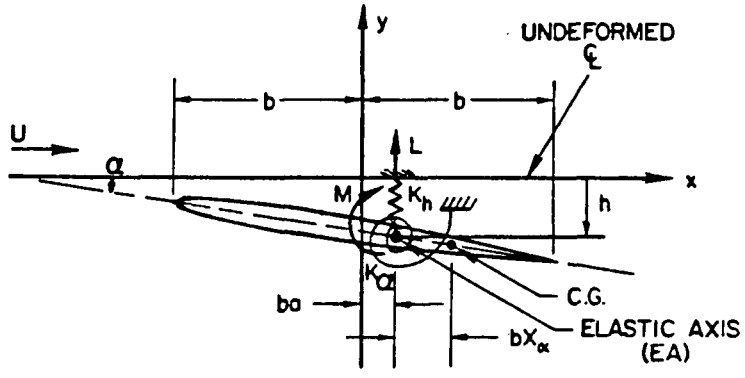

EQUATIONS OF MOTION

$$m\ddot{h} + S_\alpha \ddot{\alpha} + K_h h = -L = \frac{1}{2}\rho_\infty U_\infty^2 c^2 C_M \qquad (5)$$

$$S_\alpha \ddot{h} + I_\alpha \ddot{\alpha} + K_\alpha \alpha = M_{ea} = \frac{1}{2}\rho_\infty U_\infty^2 c\, C_L \qquad (6)$$

FIGURE 1

METHOD OF SOLUTION

Aeroelastic stability is determined by integrating the equations of motion for the coupled fluid-structure system. The structural equations are first transformed to normal coordinates η_r , Eqs. (7)-(8), where the columns of $[\Phi]$ are the eigenvectors of the free vibration problem. The structural integrator is based on the convolution integral solution, Eq. (9), and the generalized aerodynamic forces Q_r are assumed to vary linearly within each time step Δt . Because the multi-stage Runge-Kutta scheme used to integrate the unsteady Euler equations was found to be sensitive to the manner in which the airfoil boundary condition was updated and the mesh moved, the structural integrator has been imbedded within the Runge-Kutta scheme in the Euler code. This permits an efficient implementation of the exact airfoil boundary condition, Eq. (10), on the instantaneous position of the airfoil, given by $B(x,y,t) = 0$. Nonreflective boundary conditions are used in the far field.

- **COUPLED EQUATIONS FOR FLUID & STRUCTURE ARE INTEGRATED NUMERICALLY USING NORMAL COORDINATES**

$$\{q\} = [\Phi]\{\eta\} \tag{7}$$

$$\ddot{\eta}_r + \omega_r^2 \eta_r = Q_r \tag{8}$$

- **STRUCTURAL INTEGRATOR IS BASED ON CONVOLUTION INTEGRAL SOLUTION**

$$\eta_r(t) = \eta_r(0) \cos \omega_r t + \frac{\dot{\eta}_r(0)}{\omega_r} \sin \omega_r t + \frac{1}{\omega_r} \int_0^t Q_r(\tau) \sin[\omega_r(t-\tau)]d\tau \tag{9}$$

- **STRUCTURAL INTEGRATOR IS IMBEDDED IN FIVE-STAGE RUNGE-KUTTA SCHEME FOR EULER EQUATIONS**

  - **EXACT AIRFOIL B.C. IS SATISFIED**

$$\frac{DB}{Dt} = 0 \quad \text{or} \quad \frac{\partial B}{\partial t} + \vec{u} \cdot \nabla B = 0 \quad \text{on} \quad B(x,y,t) = 0 \tag{10}$$

  - **MESH IS MOVED AT EACH STEP**

NUMERICAL RESULTS

Flutter calculations have been carried out for the three aeroelastic test cases listed in Table 1, and compared to previously published calculations based on various TSD codes. Case A is the same as studied by Isogai (Refs. 5,6) and later by Edwards et al. (Ref. 7) and also by Weatherill and Ehlers (Ref. 8). Note that the elastic axis location "a" is ahead of the leading edge; the idea here is to simulate the vibratory behavior (in pitch and plunge) of the streamwise sections near the tip of a swept-back wing. Case B has been studied previously by Isogai (Ref. 6) and by Ueda and Dowell (Refs. 9,10). Case C was introduced by Ueda and Dowell as an example where nonlinear (amplitude) effects were clearly discernible, based on LTRAN2 aerodynamics implemented via the describing function method. In all cases, the airfoil is forced for 3-6 cycles in pure torsion at a reduced frequency of interest, released, and the aeroelastic equations are integrated forward in time for another 3-6 cycles. The flutter boundary is located by calculating the logarithmic decrement δ of the transient solutions, and interpolating to $\delta=0$ between adjacent solutions with different $U/b\omega_\alpha$.

TABLE 1

Aeroelastic Test Cases

Case	A	B	C
Airfoil(s)	NACA 64A010	NACA 64A010	NACA 64A006
M_∞	0.7 - 1.0	0.80	0.86
a	-2.0	-0.3	-0.3
x_α	1.8	0.5	0.5
r_α^2	3.48	0.49	0.49
μ	60	60	60
ω_h/ω_α	1.0	0.2	0.2
Refs.	5,6,7,8	6,9	10

MESH GENERATION

The unsteady Euler calculations are carried out on a C-mesh of quadrilateral elements, generated by means of a square root transformation followed by selective stretching to compress the grid near the trailing edge. A near field view of the resulting mesh is shown in Fig. 2. In the far field, the mesh extends to 15-100 chords, depending on direction. The mesh moves with the airfoil as a rigid body, i.e. without deformation. Flutter calculations published earlier by the authors (Ref. 4) were carried out on a 96 x 16 C-mesh, which was found to give adequate engineering accuracy in most, but not all, of the cases studied. In the present study, additional calculations have been performed on both 96 x 16 and 192 x 32 C-meshes, and the results of Ref. 4 have been updated where appropriate.

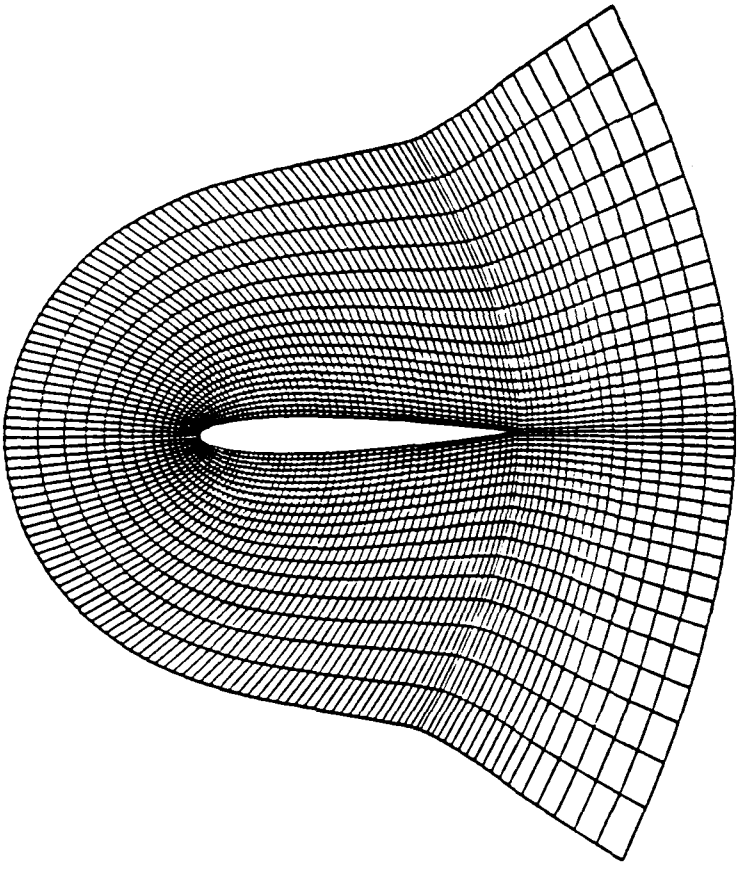

FIGURE 2

FLUTTER BOUNDARIES FOR CASE A

Previous studies (Refs. 5-8), which have been based on a number of different transonic small disturbance (TSD) theories, generally agree that the flutter boundary for Case A exhibits a significant "transonic dip", as shown in Fig. 3. Also shown in this figure are the results of flutter calculations based on the present Euler code, and using an initial forcing amplitude of 0.1 degree in pitch. Overall, the agreement with previous TSD calculations are fairly good. However, the Euler calculations appear to shift the bottom of the "bucket" toward higher Mach numbers. It is interesting to note that the bend-back of the flutter boundary around $M \sim 0.88$ observed by Edwards et al. (Ref. 6) and Weatherill and Ehlers (Ref. 8), is also predicted by the present Euler calculations. Not surprisingly, the precise location of the nose of the curve, where the flutter boundary has a vertical tangent, was found to be sensitive to the mesh size used in the calculations.

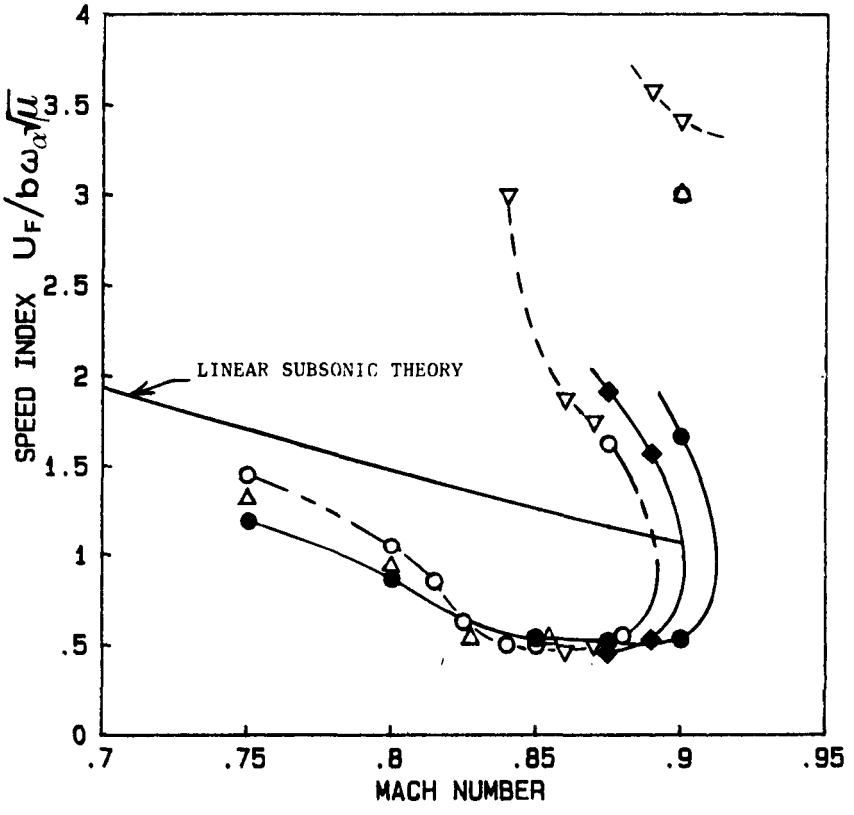

FIGURE 3

FLUTTER FREQUENCIES FOR CASE A

Figure 4 shows the flutter frequencies vs. Mach number, with some comparisons to earlier OPTRAN2 calculations by Weatherill and Ehlers (Ref. 8). As first noted by Isogai (Ref. 5), the flutter mode is essentially the first (predominantly bending) natural mode. The flutter frequency is close to the first coupled natural frequency ω_1/ω_α until the nose of the bend-back is encountered. At this point, the flutter frequency increases to a value between the two coupled natural frequencies and the flutter mode also changes, although it is still associated with the first predominantly bending branch.

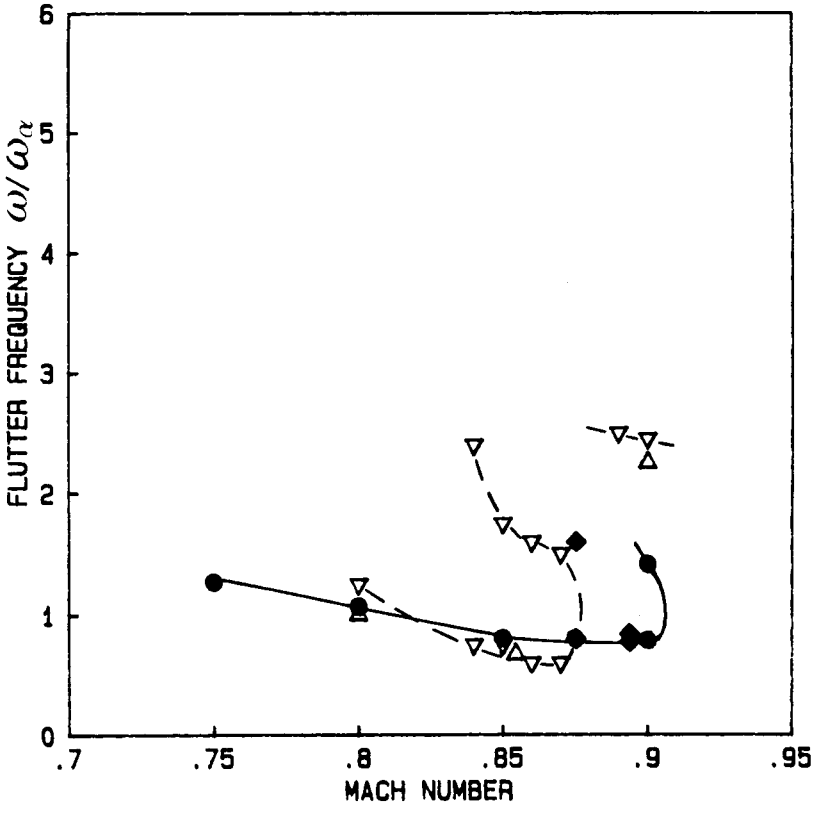

FIGURE 4

TRANSIENT SOLUTIONS FOR CASE A AROUND LOWER FLUTTER BOUNDARY AT M = 0.9

Typical transient solutions for Case A are shown in Figs. 5,6. At a Mach No. of 0.9, multiple flutter solutions occur due to the bend-back of the flutter boundary (see Fig. 3). Figure 5 illustrates the dynamic behavior of the airfoil, plotted as $h(t)/b$ and $\alpha(t)$ vs. time, immediately above and below the lower flutter point at $M = 0.9$. In this case, the airfoil is stable below (bottom figure) and unstable above (top figure) the neutral stability boundary ($\bar{U}_F = U_F/b\omega_\alpha$ vs. M.) Here, the airfoil has been forced for 3-6 cycles in pure pitch, with an amplitude of 0.1°, and then released at t=0.

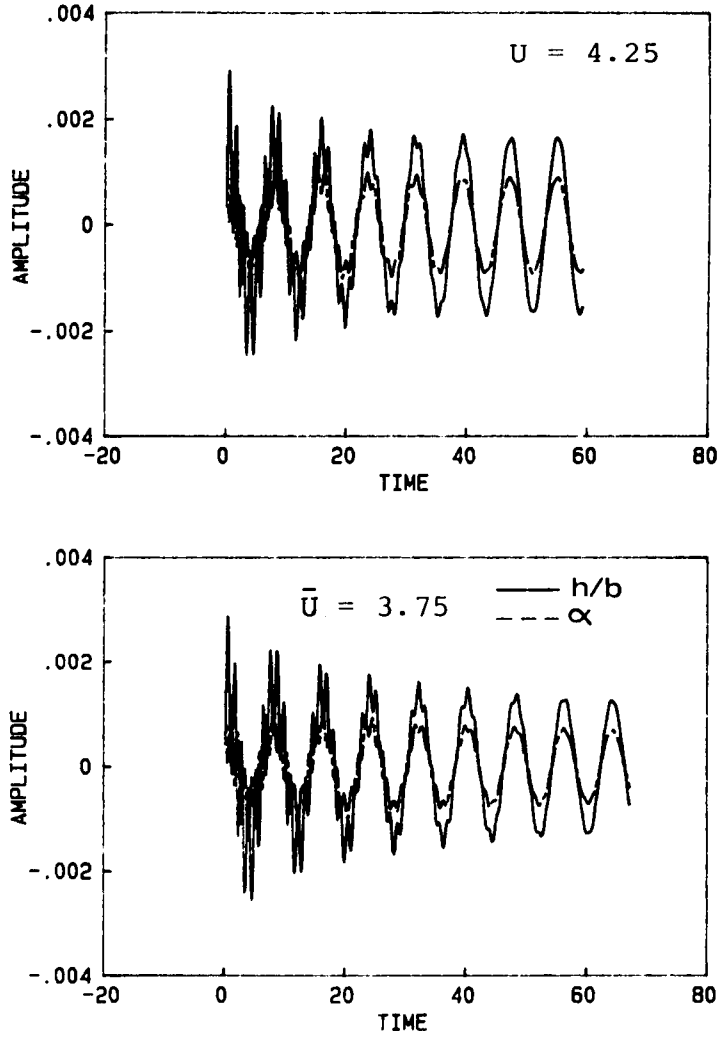

FIGURE 5

TRANSIENT SOLUTIONS FOR CASE A AROUND UPPER FLUTTER BOUNDARY AT M = 0.9

In the vicinity of the upper flutter point at M = 0.9, the stability behavior is reversed from that observed around the lower point. The airfoil is now stable for values of nondimensional airspeed $U/b\omega_\alpha$, above the neutral stability boundary, as shown in the bottom diagram of Fig. 6. Conversely, the airfoil is unstable for values of $U/b\omega_\alpha$ below the flutter boundary.

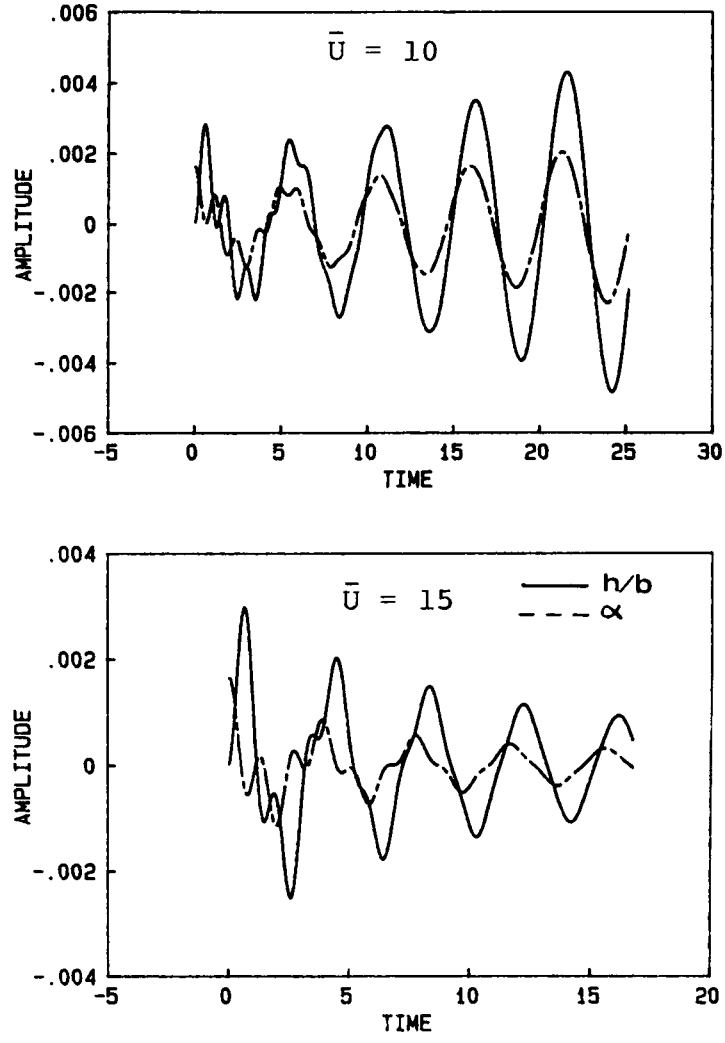

FIGURE 6

FLUTTER CALCULATIONS FOR CASE B

In Table 2, the results from our present flutter calculations for Case B are compared to predictions by previous researchers using various TSD codes. This case is the same as Case B considered by Isogai in Ref. 6. Note that the present Euler calculations predict a somewhat higher flutter speed than the TSD calculation by Isogai, but still below the speed predicted by classical linear theory. The flutter speed predicted by Ueda and Dowell (Ref. 9), using the describing function method based on LTRAN2 aerodynamics, is significantly below the predictions of the Euler code.

TABLE 2

Comparison of Predicted Flutter Speed for Case B

Method	α	$U_F/b\omega_\alpha$	$2k_F$
Present	0.1°	3.43	0.201
Ueda & Dowell[9]	0.25°(ϕ_1)	2.95	0.221
Isogai[6]	0.1°	3.25	0.215
Linear Theory	-	3.86	0.210

NONLINEAR DEPENDENCE OF FLUTTER SPEED ON INITIAL FORCING AMPLITUDE FOR CASE C

In Refs. 9-10, Ueda and Dowell investigated the nonlinear amplitude dependence of the flutter boundary for Case C, Table 1. They found a distinct drop in the flutter speed as the amplitude of the effective induced angle of attack $\phi_1 = \alpha + \dot{h}_c/U$ exceeded about 1°, where $\dot{h}_c$ is the plunging velocity at midchord. Figure 7 shows results from the present Euler calculations, plotted as flutter speed vs. initial forcing amplitude in pitch (prior to release). Note that the flutter boundary is not very sensitive to α in the range 0°-5°, and that the results obtained are sensitive to the initial forcing frequency.

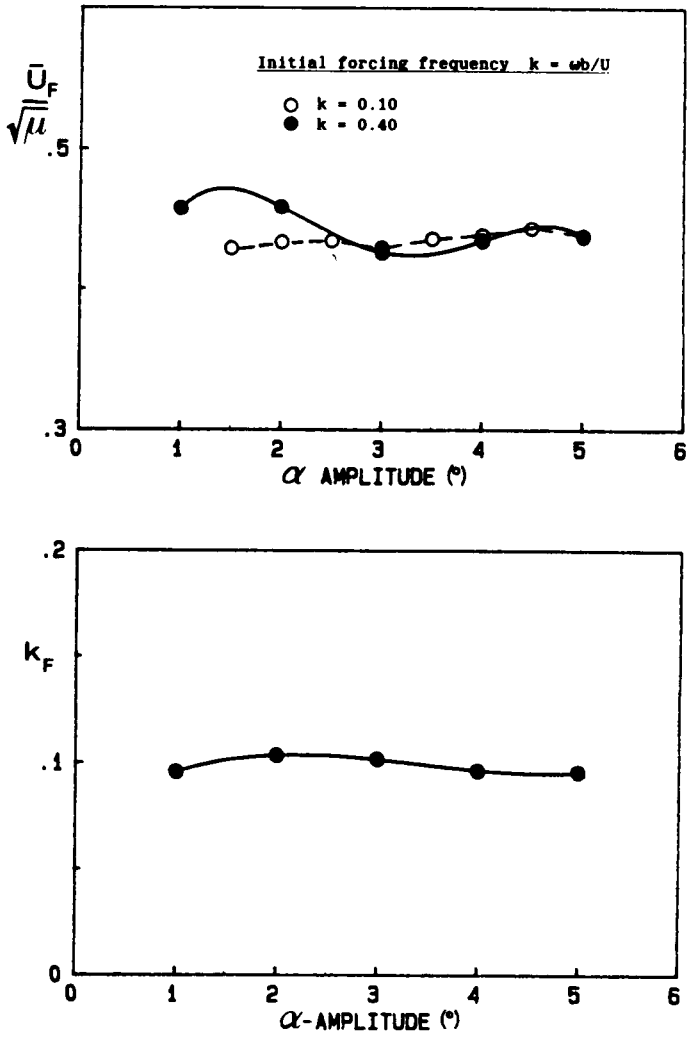

FIGURE 7

TRANSIENT SOLUTIONS FOR CASE C

Typical stable and unstable transient solutions are shown in Figs. 8 and 9, corresponding to initial forcing amplitudes of $\alpha = 1°$ and $4°$, respectively. The flutter mode is again a predominantly bending mode and emerges quickly (within a couple of cycles), despite the fact that the initial disturbance is pure torsion. This rapid convergence toward the significant aeroelastic mode was also observed in most of the transient solution of Cases A and B as well.

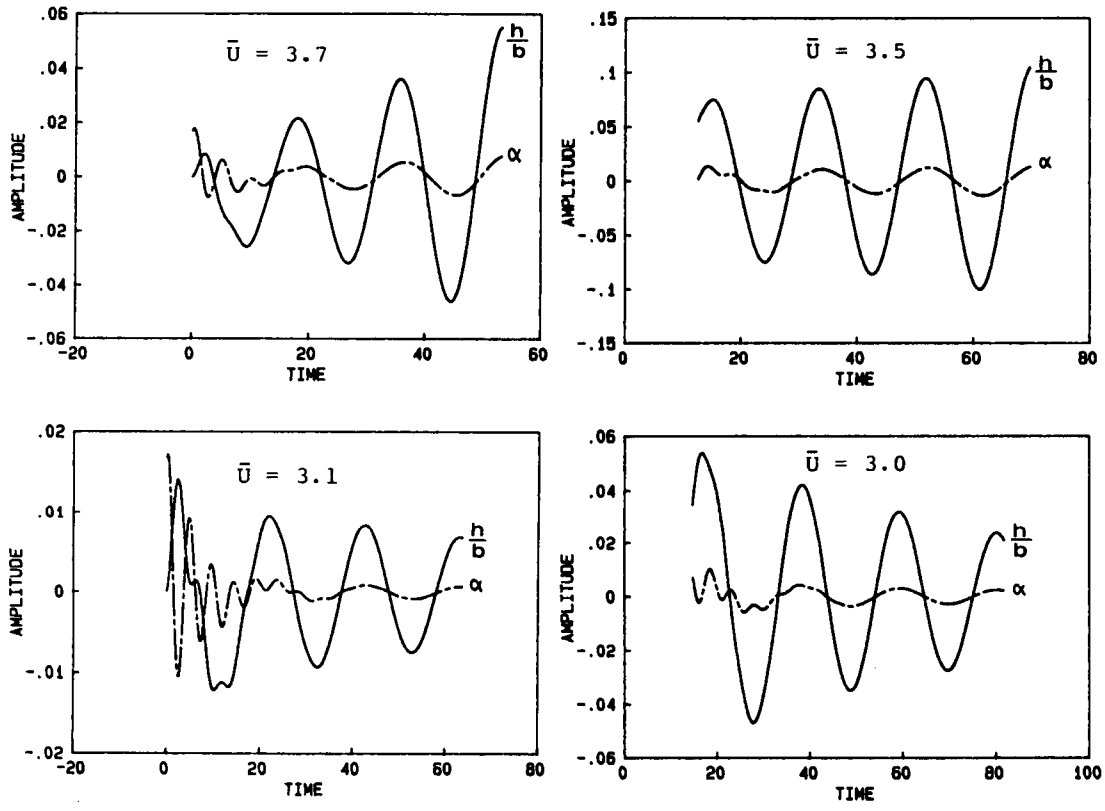

FIGURE 8

FIGURE 9

CONCLUSIONS

1. Typical section flutter calculations based on the two-dimensional unsteady Euler equations are now feasible.

2. Flutter speeds predicted by the present Euler code are in good overall agreement with previous TSD calculations, except in cases where strong shocks are present.

3. The Euler code calculations predict a transonic dip similar to the corresponding dips predicted by TSD codes, but shifted toward higher Mach numbers.

4. Multiple flutter points occur at certain Mach numbers, caused by a bend-back of the flutter boundary.

5. The amplitude dependence of U_F appears to be less than might be expected.

REFERENCES

1. Ashley, H., "Role of Shocks in the 'Sub-Transonic' Flutter Phenomenon," Journal of Aircraft, Vol. 17, March 1980, pp. 187-197.

2. Jameson, A. and Venkatakrishnan, V., "Transonic Flows About Oscillating Airfoils Using the Euler Equations," AIAA Paper No. 85-1514-CP, July, 1985.

3. Venkatakrishnan, V., "Computation of Unsteady Transonic Flows Over Moving Airfoils," Ph.D. Dissertation, Dept. of Mechanical and Aerospace Engineering, Princeton University, Oct. 1986.

4. Bendiksen, O.O. and Kousen, K.A., "Transonic Flutter Analysis Using the Euler Equations," AIAA Paper No. 87-0911-CP, April, 1987.

5. Isogai, K., "Transonic Dip Mechanism of Flutter of a Sweptback Wing: Part II," AIAA Journal, Vol. 19, Sept. 1981, pp. 1240-1242.

6. Isogai, K., "Numerical Study of Transonic Flutter of a Two-Dimensional Airfoil," NAL TR-617T, National Aerospace Institute, Tokyo, Japan, 1980.

7. Edwards, J.W., et al.,"Time-Marching Transonic Flutter Solutions Including Angle-of-Attack Effects," Journal of Aircraft, Vol. 20, Nov. 1983, pp. 899-906.

8. Weatherill, W.M. and Ehlers, F.E., "A Three Degree-of-Freedom, Typical Section Flutter Analysis using Harmonic Transonic Air Forces," AIAA Paper No. 83-0960, May, 1983.

9. Ueda, T. and Dowell, E.H., "Flutter Analysis Using Nonlinear Aerodynamic Forces," Proc. AIAA/ASME/ASCE/AHS SDM Conf., New Orleans, LA, May 1982, pp. 462-481.

10. Ueda, T. and Dowell, E.H., revised and extended version of Ref. [9], Journal of Aircraft, Vol. 21, No. 2, Feb. 1984, pp. 101-109.